Quantum Wires and Quantum Dots in Heterojunction Devices with Field-Effect Electrodes

W. Hansen, D. Schmerek and H. Drexler*
Ludwig-Maximilians-Universität, Müchen
Geschwister-Scholl Pl. 1, 80539 München, Germany

Received July 21, 1995

We generate in especially designed heterojunction crystals one-dimensional electron wires and zero-dimensional electron dots with a field-effect controlled number of electrons occupying the lowest quantum states. Very strong and well controlled confinement of one-dimensional quantum wires is achieved with patterned field electrodes, that allow us to study the electronic properties of quantum wires as function of the stiffness of the confinement potential. For experiments on smallest electron dots with very large energy spacing of the quantum dot levels we study structurally confined electrons in self-assembled InGaAs islands that are grown in the Stranski-Krastanow mode. The electron systems are characterized with capacitance spectroscopy and with far-infrared absorption experiments that probe the electronic ground states and the fundamental excitations, respectively.

I. Introduction

Many physical properties of an electron system are critically dependent on its dimensionality. This is mainly due to modified screening and diffusion and the reduced density of states (DOS) in lower-dimensional electron systems. The latter arises from the fact that confinement of the electrons reduces the degree of freedom for free motion and thus the dimensionality of the quasi-continuous regions in phase space. Thus energy levels of electron systems confined in one or two dimensions form two- or one-dimensional subbands. Of course, confinement into all three spatial dimensions leads to a fully quantized energy spectrum like in an atom. So-called two-dimensional electron systems are usually generated in the plane of a semiconductor-insulator or semiconductor heterojunction interface and are well known for more than three decades[1]. The tunability of the electron density as well as the advantages associated with the reduced dimensionality have given rise to a vast number of technological applications among which the best known are field effect transistors and heterostructure lasers[2].

Within the last decade growing interest has been devoted to the fundamental properties of one- and zero-dimensional electron systems, so-called quantum wires or quantum dots[3]. Such systems are preferentially prepared from a high mobility two-dimensional electron system at the interface of a modulation-doped heterojunction crystal. Their geometry is usually defined either by etching patterns into the crystal surface or by means of patterned field-effect electrodes biased to deplete the areas beneath the electrodes of mobile electrons[4]. Then electron stripes or discs are left in the unetched areas or in the gaps between the electrodes. Although these techniques have become quite sophisticated and many intriguing results are obtained, important parameters like the energy quantization due to the lateral confinement and the number of electrons occupying the one-dimensional subbands of the wires or the energy levels of the dots is often not well known and determined quite indirectly if at all. Furthermore, the influence of the density of states on transport and optical properties is quite involved, so that in general it is impossible to determine this fundamental quantity from such experiments. For instance, in transport experiments electron localization and in optical transitions selection rules as well as collective effects are important aside from pure density of states effects.

The experiments on quantum wires and quantum dots described in the following are performed with

*present address: Center for Free Electron Laser Studies, University of California, Santa Barbara.

devices especially designed to have very well defined, strong confinement and a good control of the electron density. We present capacitance spectra that clearly reflect the quantization of the electronic energies due to the lateral confinement. Indeed, capacitance spectroscopy has previously been very successfully applied to two-dimensional electron systems in order to obtain information about the two-dimensional thermodynamic DOS[5–8]. There with a refined method[7] it was even possible to determine quantitatively many-particle corrections to the single particle DOS, which are found to be very important at small electron densities or in high magnetic fields. For technical reasons, that will become obvious in the following, this refined method cannot be applied to one- or zero-dimensional electron systems and a sophisticated quantitative analysis is only possible with self-consistent numelical calculations basing on parameters that are less well controlled. Nevertheless, the substructures observed in the differential capacitance can be interpreted on basis of very simple models yielding a good notion about important parameters such as quantization energies, electron occupation and typical widths of the structures. Furthermore, the electron wires realized in our experiments are of such good quality, that unlike in previous experiments the substructures are clearly observed in the direct capacitance signal rather than in the derivative making a comparison to self-consistent numerical calculations less ambiguous.

The parameters obtained from the capacitance spectra are used to understand the high frequency conductivity of the quantum wires. These exhibit characteristic resonances in the Far-Infrared (FIR) that are associated with transitions between the one-dimensional subbands of the wire or the energy levels of the dot. Comparison of the subband spacing extracted from the capacitance data to the resonance energies tells us about the collective contributions to the intersubband transitions, and in the case of the quantum dots it substantiates our interpretation of the capacitance data.

II. Samples

The samples of our experiments are basically metal-insulator heterojunction (MIS) diodes[9]. The heterojunction is grown by molecular beam epitaxy. A typical epitaxial layer sequence and an idealized band structure are sketched in Fig. 1a and 1b. On the [100] surface of a GaAs substrate wafer an undoped GaAs buffer, a highly doped GaAs layer with typical thickness of 20 nm, an undoped GaAs spacer layer and an undoped barrier layer are grown. The highly doped GaAs contains an electron system of low mobility, which is conducting (sheet conductivity typical $\sigma \approx$10mS) even at the low temperatures and high magnetic fields of our experiments. It forms a back electrode buried in the heterostructure sample. The front barrier is made of an undoped short period AlAs/GaAs superlattice (SPS), each layer typically 10 epitaxial monolayers thick. Such a barrier exhibits a low leakage current and serves here as an undoped insulator. The thickness of the SPS is typically 32 nm and covered with a 10 nm thick undoped GaAs layer to protect the AlAs against oxidation. On this heterojunction crystal a metal gate (typically 30 nm Ti) is thermally evaporated.

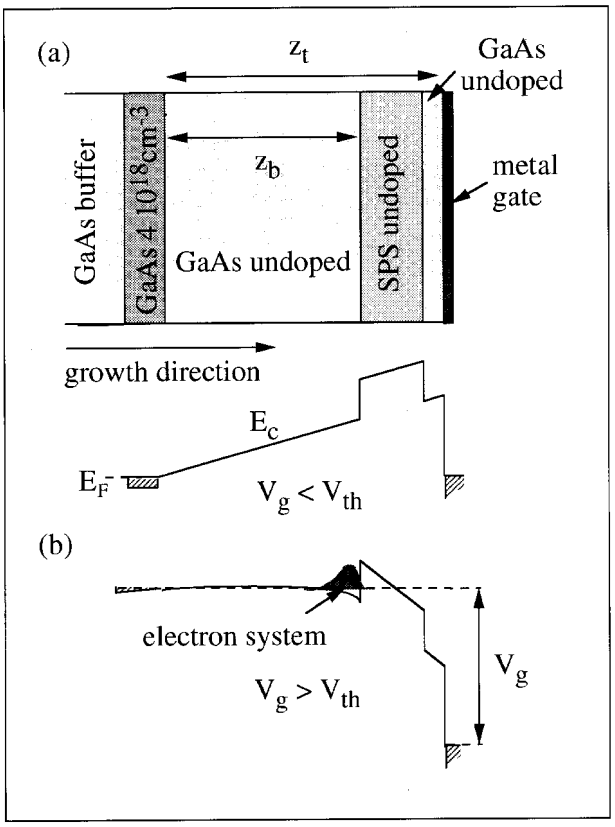

Figure 1. (a) Cross section through the epitaxially grown layers of a MIS-diode. The distances between back electrode and heterojunction interface z_b as well as top gate z_t are indicated. The thickness of the GaAs spacer layer on top of this electrode is typically $z_b = 100$ nm. (b) Sketch of the conduction band edge as function of the coordinate in growth direction at gate voltage below and above a threshold voltage Vtll as described in the text.

Note that unlike in a conventional modulation-doped[10] heterojunction our MIS- diodes generally do

not contain mobile electrons at the heterojunction interface at zero gate voltage as indicated in Fig. 1b. Like in a Si metal-oxide-semiconductor diode the carriers have to be field induced by a positive gate voltage applied between the back electrode and the front gate. If the gate voltage V_g is larger than a threshold voltage V_{th} the conduction band edge forms a minimum at the interface between the GaAs spacer layer and the front barrier into which electrons are injected from the back electrode. In all experiments discussed in the following charge injection through the shallow tunnel barlier formed by the undoped spacer layer happens sufficiently fast that we can assume equilibrium with respect to charge exchange between the electron system at the heterojunction interface and the back electrode. The advantage of our MIS-diodes is that no intentional dopants are contained in the layers between the field induced electron system and the front gate. This is important if we want to generate very small electron systems with high mobility and precisely controlled, strong lateral geometry at the heterojunction interface. In a conventional modulation-doped heterostructure large areas would have to be depleted from mobile electrons in order to define small electron wires or dots. The remaining dopants in the front barrier are left unscreened and thus seriously deteriorate the potential in the wires or dots[11].

Beneath a homogenous large gate electrode a two-dimensional electron system is formed at the heterojunction interface at $V_g > V_{th}$. If the gate is patterned in the plane of the crystal surface the geometry of the electron system will represent an according replica of this pattern. In Fig. 2 the gate pattem, that we use for the generation of field-induced quantum wires, is depicted together with the back electrode. The so-called interdigital gate consists of two electrodes that can be biased at different voltages with respect to the back elect ode. As indicated in Fig. 2 they form a grating of parallel metal stripes with every second stripe biased at a voltage V_g with respect to the back electrode and with a voltage difference V_d to the adjacent stripes. We define the geometry of our interdigital gates by electron beam lithography with a bilayer PMMA resist. The metal stripes are prepared by thermal evaporation and a lift-off process. As indicated in Fig. 3 the width of the metal stripes is 100 nm, the gap between adjacent stripes is 150 nm so that at $V_d \neq 0$ the period of the surface potential is a=500 nm.

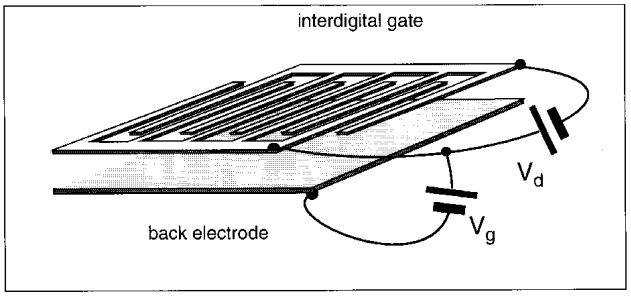

Figure 2. Sketch of the electrode configuration for the generation of field-induced quantum wires. The gate voltage V_g is applied between the back electrode in the heterostructure crystal and one of the interdigital electrodes. The voltage V_d is applied between the two interdigital electrodes.

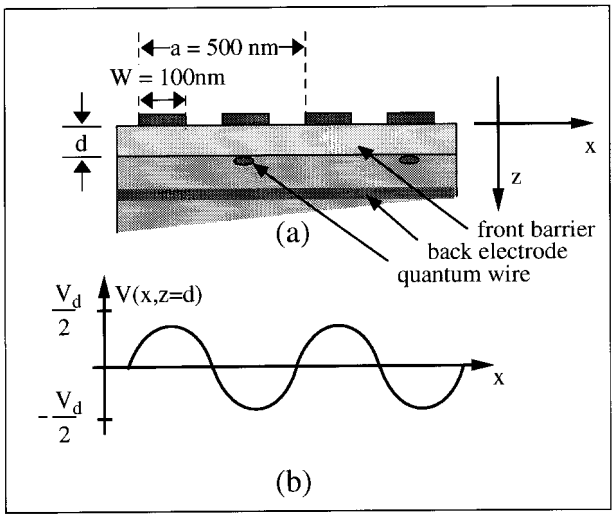

Figure 3. (a) Cross section through a MIS-diode with an interdigital gate. (b) Potential superlattice induced by the interdigital gate in the plane of the heterojunction interface. Electrons are injected from the back electrode into the potential minima if the gate voltage V_g is sufficiently high. The corresponding location of the electron wires is indicated in (a).

The interdigital gate offers a good control of the periodically modulated surface potential of our heterojunction devices. At the open crystal surface in the gaps between the metal stripes the surface potential is not well known. The unknown boundary conditions for the open surface regions cause considerable arbitrariness in model calculations of the potential beneath split gate devices[12,13] However, with split gate devices the modulation amplitude of the surface potential is fixed, if stress effects[12] caused by different

thermal contraction of the electrode and semiconductor material can be neglected. In Fig. 3 a cross section through a MIS-diode with a interdigital gate and the superlattice potential in the plane of the heterojunction interface are indicated. The Fourier components of the surface potential decay rapidly in the z-direction according to $sinh[q(z_t-z)]/sinh[qz_t]$. Here $q = n2\pi/a$, $(n = 1, 2, ...)$, is the wave vector of the corresponding Fourier component and z is the distance of the plane in which the superlattice potential is calculated from the plane of the gate. However, since in our structures the distance $d = z_t - z_b$ between the heterojunction interface and the surface is small (typically $d = 40$ nm) a considerable fraction of the modulation amplitude is still present in the plane of the electron system. We estimate that the first Fourier component of the unscreened superlattice potential is reduced by about 50% at the heterojunction interface. At this point it becomes apparent that modulation doped heterojunctions with very large spacer layers in the front barrier to preserve high mobility even at low densities are inadequate for our purposes. The separation between the planes of the electron system and the front gate would be too large to ensure strong potential modulation.

Thus the amplitude of the superlattice potential is controlled by the voltage V_d as long as the potential landscape at the heterojunction interface is not filled with electrons. The gate voltage V_g controls the alignment of the potential landscape with respect to the Fermi energy in the back electrode. Once the potential minima are filled with electrons as indicated in Fig. 3 the external potential induced by the gate electrodes is partly screened. The distinction between the so-called *bare* potential induced by the external electrodes and the *effective* potential, that includes the electron-electron interaction and thus determines the subband spacing, will become important for the discussion of the high frequency response of the quantum wires.

Although zero-dimensional electron discs can be also defined by pure field effect[14] we shall discuss in the following a recently employed method[15] to generate extremely small quantum dots that takes advantage of the so-called Stranski-Krastanow growth modus. Here a coherently strained InGaAs layer is grown on top of the undoped GaAs spacer layer of our MIS-diodes, as is depicted in Fig. 4[16]. It is well known that the growth of a strained InGaAs layer on a GaAs substrate leads to spontaneous formation of semiconductor islands with very small sizes. This so-called Stranski-Krastanow growth mode emerges after growth of a few monolayers as is judged by the reflection high-energy electron diffraction (RHEED) pattern[15]. At this point the InGaAs layer spontaneously relaxes into dislocation free, lens-shaped InGaAs islands randomly distributed and embedded in a very thin InGaAs wetting layer. Inspection with scanning an atomic force microscope (AFM) and a transmission electron microscope (TEM) reveal that at optimized growth conditions the islands have a diameter of typically 20 nm in the plane of the wetting layer and are about 6 nm high in the direction perpendicular. Furthermore, it is found that the size distribution is remarkably narrow with the diameter fluctuating only by about 10% and the height by only one monolayer[15,17]. The dot densities are adjustable between typically 10^9 cm^{-2} and several 10^{10} cm^{-2}.

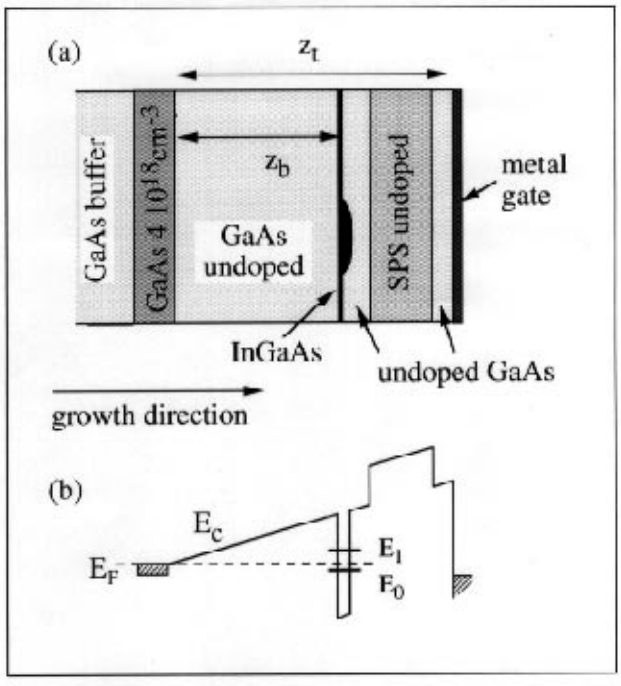

Figure 4. (a) Cross section through a MIS-diode containing a thin InGaAs quantum well with lens shaped Stranski-Krastanow islands at a distance z_b from the back electrode. (b) Conduction band edge along a line in the growth direction that intersects the InGaAs-island of the structure in (a). Two energy levels are indicated schematically in the quantum well of the InGaAs-island.

After formation of the InGaAs islands a 5 nm thick GaAs spacer layer is deposited before the growth is fin-

ished with the SPS barrier and the cap layer of the MIS-diode. Here the GaAs acts like a barrier in which almost ideal type I InGaAs quantum boxes are embedded. As will be demonstrated in the following the occupation of the electronic energy levels in the InGaAs dots can be nicely controlled by means of the gate bias applied between the homogeneous front gate and the back electrode of our MIS-diodes.

III. Experiments

We would like to first discuss capacitance measurements on quantum wires defined with interdigital gates. In Fig. 5 we depict typical results[18] obtained on a MIS-diode with d=42 nm and z_t=142 nm. Each electrode of the interdigital gate consists of 300 stripes. Each stripe is 180 μm long. Stripe width W and period a are as indicated in Fig. 3. The differential capacitance is measured by slightly modulating the voltage Vg at a frequency f=lOkHz and with an amplitude of dV = 5 mV. The differential capacitance is calculated from the excited ac current through the sample.

If all the electrodes involved would be perfectly metallic the capacitance would be entirely determined by the geometric arrangement of the electrodes. In our case, however, the center electrode formed by the one-dimensional wires is not perfectly screening the electric field due to the finite DOS in the electron system. To charge the wires with electrons the conduction band edge has to be lowered so that the electrochemical potential of the electron wires is kept aligned with the chemical potential in the back electrode. Consequently, net charge has to be simultaneously induced in the back electrode and an electric field is maintained between the back electrode and the wires. The device capacitance thus deviates from the value that pure metallic electrodes would have. This fact is well known from similar measurements on two-dimensional electron systems,[5-8] where e g. in a magnetic field the formation of Landau levels in the DOS is clearly reflected. In the reduced DOS between the Landau levels results in pronounced minima of the capacitance signal at integer filling factors.

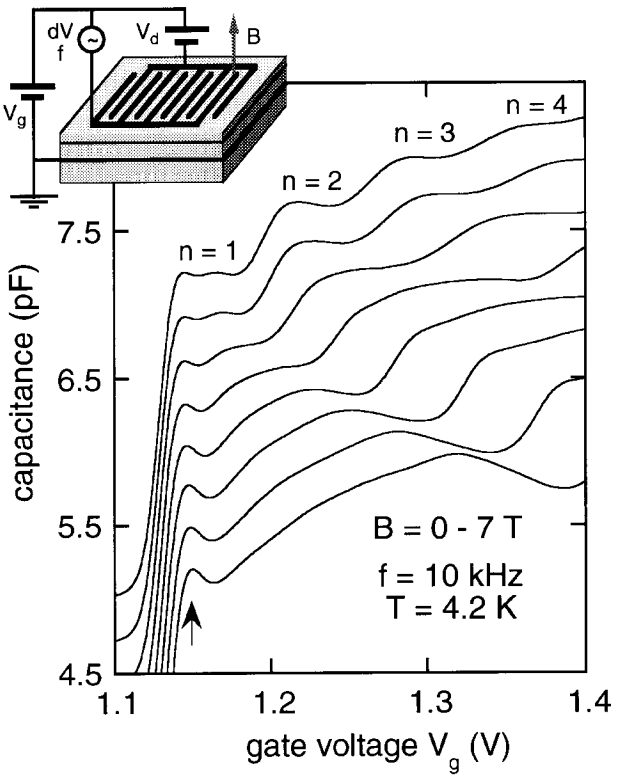

Figure 5. Capacitance of a wire array as function of the gate voltage V_g. The experimental arrangement is indicated in the inset. Different traces have been recorded at different magnetic fields applied pelpendicular to the sample surface. The capacitance scale refers to the top trace that has been recorded at zero magnelic field. The field has been increased in steps of 1 T in the lower traces, which are offset for clarity. The voltage bias between the electrodes of the interdigital gate is V_d=1.0 V. As described in the text the indices at the top trace denote the one-dimensional sub-bands that are filled in the corresponding gate voltage ranges. A substructure in the spectra, that is discussed in the text, is highlighted by an arrow. (From Ref.[18]).

We thus expect that the capacitance signal in Fig. 5 reflects the density of states of the one- dimensional subbands in the wire. At the threshold voltage $V_g = V_{th} \approx 1.13$ V the capacitance signal increases rapidly, reflecting the generation of the quantum wires which represent a third electrode between the front gate and the back electrode. At larger gate voltages pronounced structures are apparent even if no magnetic field is applied. The strong steps numbered with indices in Fig. 5 reflect the one-dimensional subband onsets as can be verified by their dependence on the voltage difference V_d and on a magnetic field applied perpendicular to the wires. A straight forward quantitative analysis of the capacitance data at zero magnetic field is hampered in our case by the fact, that a parasitic capacitance between the front electrode and the back contact con-

tributes to the signal even when the electron wires are formed. We expect the wires to widen with increasing electron occupation, so that the parasitic capacitance as well as the geometric contribution of the wire capacitance are not constant when the gate voltage is changed. Indeed, the overall increase of the capacitance signal in Fig. 5 reflects this behavior. Hence, the capacitance can only be modelled with a self-consistent numerical calculation that still needs to be performed.

However, a simple model can be applied to approach a quantitative analysis from the magnetic field dependence of the capacitance data. We assume that the effective confinement potential $V(x)$ in the lateral direction can be described by a harmonic oscillator potential with characteristic frequency Ω : $V(x) = m^*\Omega^2 x^2/2$. Here $m^* = 0.07 m_e$ is the effective conduction hand mass in GaAs. Furthermore, we assume that this effective confinement potential does not change considerably in the density range where only the lowest one-dimensional sub-band is occupied. Accordingly, we derive the number n_{ql} of carriers that has to be filled into the lowest one-dimensional subband when the chemical potential crosses the onset of the second subband from the ideal single particle DOS

$$n_{ql} = \frac{g_s}{\pi}\sqrt{\frac{2m^*}{\hbar}}\frac{\omega^{3/2}}{\Omega} \ ,$$

where $g_s = 2$ is the spin degeneracy of the GaAs conduction band. The separation between the first and the second one-dimensional subband increases with magnetic field according to $\hbar\omega = \hbar(\Omega^2 + \omega_c^2)^{1/2}$, and $\omega_c = eB/m^*$ is the cyclotron frequency. The steps in the capacitance signal at least partly arise from the DOS maxima at the subband edges. Since both the subband separation and the DOS within the subbands rise with the magnetic field it is plausible that the voltage separation between the subband onsets also increases with the magnetic field.

Assuming that the wire capacitance CW per unit length does not change in the densily range considered we also have $n_{ql} = c_w U_{ql}$, where U_{ql} is the separation between the onset voltages of the first and the second one-dimensional subbands. The magnetic field dependence of the voltage difference between the subband onsets thus can be described by

$$U_{ql}^{4/3} = \alpha^{4/3}(\Omega^2 + \omega_c^2) \ ,$$

where $\alpha = e g_s \sqrt{2m^*/\pi^2\hbar}/c_w\Omega$. In Fig. 6 the experimental values obtained on a sample with different voltages V_d applied between the electrodes of the interdigital gate are presented together with best fits to the data according the above equation. As expected at zero magnetic field the voltages U_{ql} increase with increasing V_d, i. e. with increasing stiffness of the confinement potential. The data are surprisingly well described by the above model even at high magnetic fields. From the fits to the data we derive subband spacings, which are depicted in the inset of Fig. 6, and a wire capacitance of $c_w = 150 pF/m$, which does not change significantly with V_d.

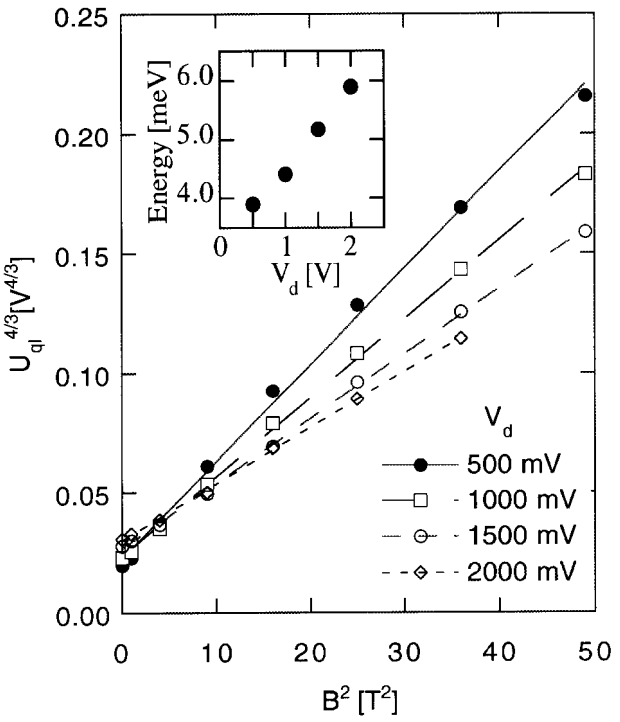

Figure 6. Experimental data of the voltage differences U_{ql} between the onsets of the first and the second one-dimensional subband in a quantum wire array measured with different voltages V_d applied between the electrodes of the interdigital gate. The exponents of U_{ql} and B are chosen such that from a simple model described in the text a linear relation is expected. Best fits to the model are depicted by straight lines. The inset shows the subband spacings obtained from the fits to the model.(From Ref.[19]).

As apparent from the inset of Fig. 6 the subband spacings increase linearly with V_d with a slope of 1.4 meV/V. Surprisingly, the extrapolation of the data to zero gate voltage gives a finite energy of 3.2 meV rather than zero. At present this result is not

understood. It may indicate non-parabolicity of the effective confinement potential or a finite potential modulation at $V_d = 0$. Such a potential may arise from charges trapped in the gaps of the interdigital gate or from stress effects[12].

Reduction of the temperature at which the capacitance is recorded to 100mK does not alter the spectra significantly except that the spin polalization of the subbands becomes noticeable at smaller magnetic fields[19]. Clearly the experimental capacitance spectra are broadened and do not reflect the singularities of the ideal one-dimensional single particle DOS. Impurities as well as inhomogeneities of the confinement potential may considerably broaden the DOS. Indeed, the overall length of the wire probed in Fig. 5 is about 5.4 cm and it is interesting to investigate how the spectra might alter, if the length of the wire is considerably reduced. A 5.4 cm long wire has been used for the experiment in Fig. 5 to guarantee a large signal to noise ratio and to reduce the influence of parasitic contributions to the signal from the measurement setup. Fig. 7 demonstrates, however, that it is possible to record with a refined measurement technique capacitance spectra on wires with length that is reduced by more than a factor of 300. Here the capacitance signal is detected with a bridge arrangement using an unbiased MIS-diode as reference. In order to minimize the influence of parasitic capacitances the signal is picked up with an impedance transformer mounted very close to the sample. A similar technique has been used by Ashoori and co-workers to measure capacitance spectra of a single quantum dot[20].

Metal stripes enclosed in tuning-fork shaped electrodes form the gate of the sample in Fig. 7. The tuning fork is biased by the voltage $-V_d$ with respect to the stripes to control the confinement potential. In spite of the considerable reduction of the wire length the spectra of Fig. 7 are qualitatively very similar to those in Fig. 5. Obviously, the mechanisms that lead to a broadening of the capacitance traces act on a length scale below 100 μm, whereas fluctuations on a macroscopic length scale do not play a significant role. Aside from the very pronounced signatures of the size quantization this proves the high quality and homogeneity of our MIS-diodes with interdigital gates.

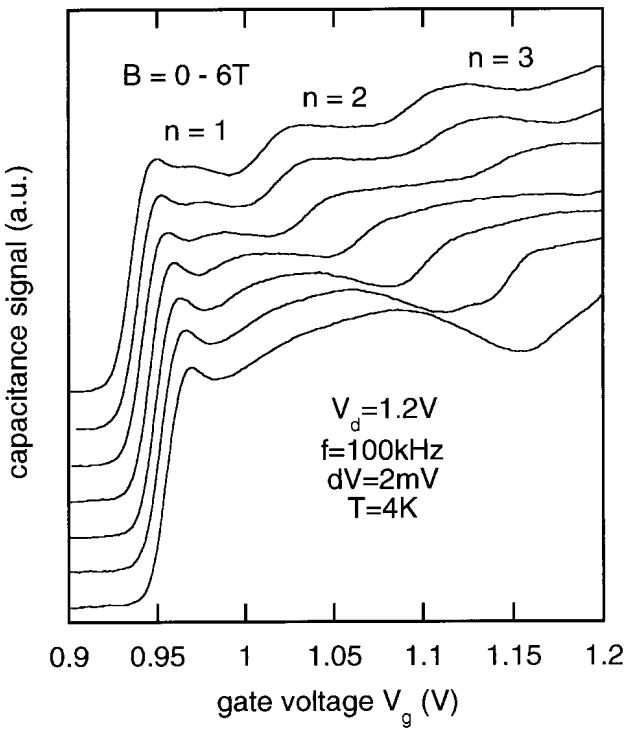

Figure 7. Capacitance spectrum recorded on a wire of 150,um length. Here the signal was recorded in a capacitance bridge arrangement with an impedance transformer attached close to the sample. The steps at the threshold voltage $V_{th} \approx 0.95$ V correspond to an increase of the capacitance of about $(8 \pm 2) fF$. The top trace is recorded at B=0, the magnetic field is increased in the lower traces in steps of 1 T. The traces are offset for clarity.

We would like to note, that in Fig. 5 as well as in Fig. 7 a substructure is clearly visible in the capacitance spectra which has not been discussed so far. It occurs close to the threshold voltage in the one-dimensional quantum limit, i. e. at gate voltages, where only the lowest one-dimensional subband is occupied. Such a substructure is not observed on two-dimensional electron systems generated, e. g., in MIS-diodes with a homogeneous gate. It becomes more pronounced at higher magnetic fields as is obvious in both figures. Spin splitting can be excluded as origin of the structure. At fields beyond 7T an additional structure arises at higher gate voltages, that can consistently be associated to the spin polarization of the one-dimensional subbands[18]. Reduction of the temperature does not significantly alter the substructure[19] and at higher temperatures it remains even visible when the steps arising from the size quantization are considerably temperature broadened[21]. The structure has been tentatively associated to a rapid renormalization of the wire potential once it becomes occupied,[18] but

due to lacking self-consistent calculations this interpretation remains speculative up to now[22].

From the strong size quantization velified with above capacitance measurements we expect a drastic modification of the high frequency conductivity of our wires as compared to a two-dimensional electron system. In particular, if the electric field is polarized perpendicular to the wires the conductivity is associated with transitions between the one-dimensional subbands, so that the zero frequency conductivity vanishes and resonances, so-called intersubband plasmons, are expected at finite frequencies in the FIR regime. One-dimensional intersubband plasmons have been intensively studied with conventional Fourier-transform spectroscopy on large wire arrays with an overall wire length of several dozens of meters[4,23] Hence in those experiments the wire arrays had to be fablicated with methods in which the confinement potential and the subband occupancy are less well controlled. In Fig. 8 a measurement technique is described with which we are able to perform FIR absorption spectroscopy even on our relatively small wires in interdigital MIS-diodes[24].

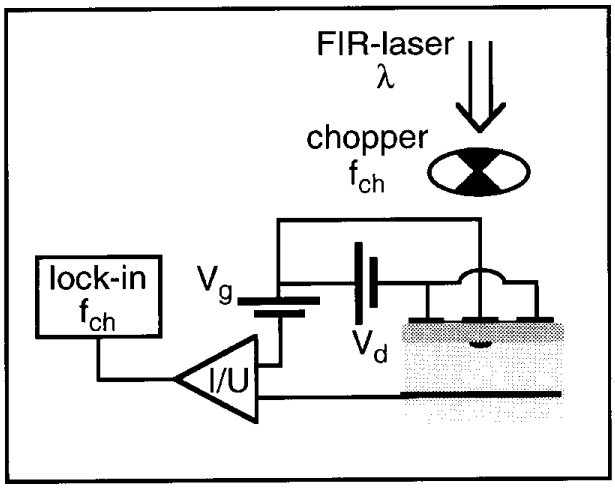

Figure 8. Measurement set-up for photo-current measurements. Charge flow from the wire system is detected with a current-voltage converter (I/U) and an amplifier (lock-in) phase locked to the modulated laser radiation.

The experimental set-up sketched in Fig. 8 resembles the set-up for measurements of differential capacitance spectra like those in Fig. 5. However, rather than modulating the gate voltage here the sample is irradiated from a FIR-laser with intensity-modulated radiation. The sample is effectively heated by the absorbed FIR if the laser wavelength is in resonance with an elementary excitation in the electron system. If the relaxation time for heat conduction from the electron system into thermal baths like the sample substrate or contacts is sufficiently long, a significant modulation of the temperature in the electron system will occur. This results in charge flow, if the thermodynamic density of states is not constant.

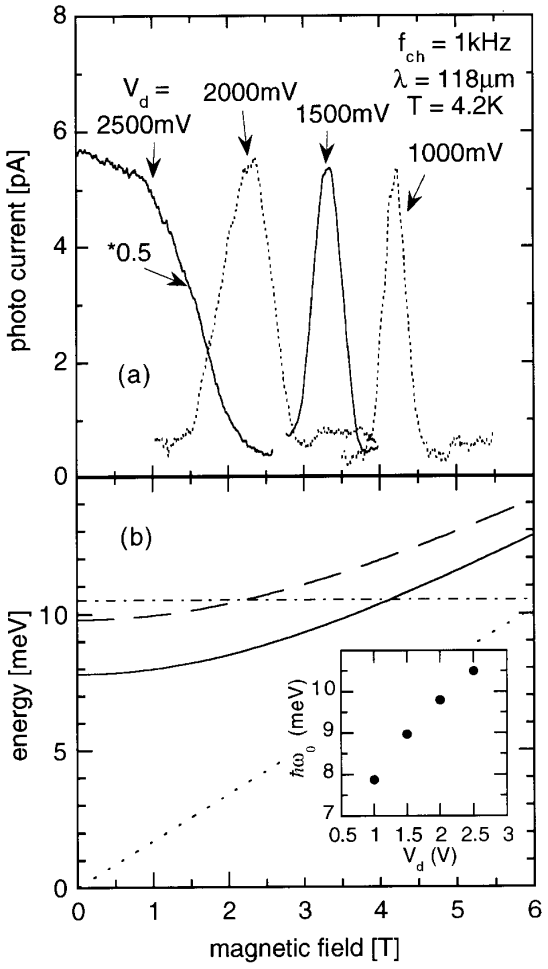

Figure 9. (a) Far-infrared absorption as function of a magnetic field detected by the photo-current of a MIS-diode with interdigital gate. Different traces are recorded with different voltages V_d between the electrodes of the interdigital gate. The gate voltage V_g is adjusted close to the threshold voltage so that the quantum wires are in the one-dimensional quantum limit. The sample is illuminated with FIR radiation of constant wavelength $\lambda = 118$ μm and the magnetic field is used to tune the resonance condition to the laser frequency as indicated in (b). (b) Resonance energies calculated in a harmonic oscillator model assuming characteristic energies of $\hbar\Omega_0 = 7.8$meV, $\hbar\Omega_0$=9.8 meV and $\hbar\Omega_0$=0 for the full, the dashed and the dotted line, respectively. The dashed dotted line indicates the energy of the laser radiation. The inset presents the zero field resonance energies $\hbar\Omega_0$ derived from the experiment versus V_d.

The photo-current on the MIS-diode of Fig. 5 is depicted in Fig. 9a as function of a magnetic field applied

perpendicular to the wires[24]. The data nicely demonstrate that the photo-current is resonantly dependent on the magnetic field and the resonance condition can be tuned by the gate voltage V_d. The behavior can be most easily understood with the generalized Kohn theorem[25,26]. This theorem bases on the assumption that the bare potential, i. e. the potential induced by the extemal electrodes, is of parabolic shape. For the sake of simplicity we pursue this assumption although it is not perfectly consistent with the assumption of a parabolic elfective potential that we have used in above analysis of the magneto-capacitance data. In an electron wire confined by a parabolic bare potential the radiation field couples only to the center of mass motion whereas the intemal electron distribution of the wire remains unchanged. Consequently, the resonances are expected to behave like single particle transitions in a harmonic oscillator potential. If the bare potential is characterized by the frequency Ω_0, the magnetic field dependence of the transition energies is given by $\sqrt{\Omega_0^2 + \omega_c^2}$ as depicted in Fig. 9b. In the inset of Fig. 9 we depict the energies $\hbar\Omega_0$ as determined from the comparison of the experimental resonance positions with the intersection.s of the calculated resonance dispersions with the laser energy.

We note, that like in Fig.6 the energies almost linearly rise with the voltage V_d. However, both the zero voltage intercept of 6.2 meV and the slope of 1.7 meV/V are considerably larger than the values in Fig. 9. This is expected, since according to our models the data in Fig. 9 reflect the unscreened bare potential, whereas the data in Fig. 6 reflect the effective electron potential at a medium value of the electron density in the one-dimensional quantum limit. The bare potential and the effective potential are equal only at very small electron densities close to the threshold voltage where the Coulomb repulsion between the electrons canbe neglected. From the quantization energy $\hbar\Omega_0 = 7.8$ meV at $V_d = 1.0V$ we determine a typical wire width of 24 nm in this case. As soon as more electrons are filled into the wire the Coulomb repulsion results into an increased wire width as determined by the effective confinement potential. From the quantization energy $\hbar\Omega = 4.4$ meV we determine an effective wire width of 31 nm.

A more sophisticated model would have to start with a self-consistent electron potential and then calculate the resonance energies from the polarizability including many-particle effects[27]. It is well known from calculations in random phase approximation, that collective contributions result in significantly larger resonance energies than the single particle level spacings. This, again, is qualitatively consistent with our experimental findings. We would like to note that recent conventional FIR transmission experiments on wire arrays with non-parabolic confinement potentials have revealed that in such wires the overall magnetic field dispersion of the intersubband-plasmons still behaves similar to the dispersion in Fig 9.b[28,29] However, there are distinct magnetic field regimes, where pronounced splittings of the resonances are observed and expected from theory[28–30] Corresponding experiments on quantum wire arrays generated by interdigital gates remain to be performed in future.

Measurements of the differential capacitance have also been very successfully applied to investigate very small zero-dimensional electron systems. As described in the previous section we generate such electron dots in InGaAs islands that are randomly distributed on a plane embedded in the GaAs spacer[16]. The difference between capacitance spectra obtained on samples with and without InGaAs islands is demonstrated in Fig. 10. The broken line represents the differential capacitance of a sample with an InGaAs layer that is too thin for the relaxation in three dimensional growth, so that no InGaAs islands are formed. The capacitance signal below gate voltage V_g=0.6 V reflects the capacitance between the homogeneous top gate and the back electrode. The steep rise of the capacitance at V_g=0.65 V reflects the generation of a two-dimensional electron system at the heterojunction interface. A very similar behavior is observed in a sample containing self-assembled InGaAs dots as demonstrated by the full line in Fig. 10. In this sample an $In_{0.5}Ga_{0.5}As$ well was grown until relaxation into islands of about 20 nm diameter with a density of about 10^{10}dots/cm^2 occured. Again a rapidly increasing differential capacitance at gate voltage V=0.65 V indicates the threshold of a two-dimensional electron system. This is further verified by the Shubnikov-de Haas oscillations in the magneto-capacitance depicted in the inset of Fig. 10.

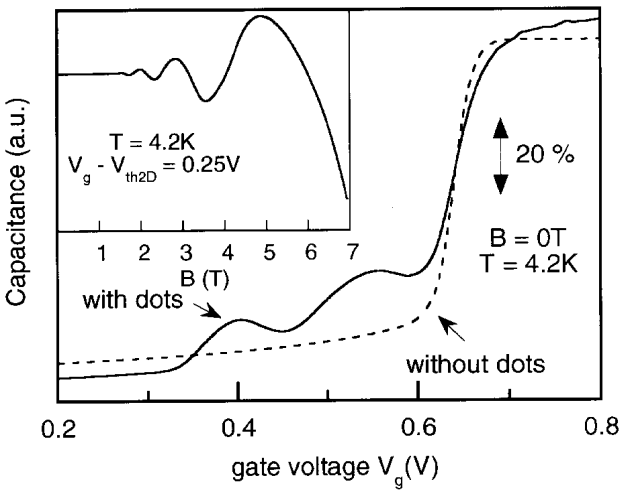

Figure 10. Capacitance spectra of a reference sample with a very thin strained $In_{0.5}Ga_{0.5}As$ layer (dashed line) and a sample containing InGaAs islands (full line). The anow denotes 20% of the capacitance between gate electrode and back electrode. The distance between these electrodes is z_t 95 nm and the InGaAs well is separated from the back electrode by z_b=50 nm. The inset depicts the magneto-capacitance of the dot-sample measured at a gate voltage beyond the threshold of a two-dimensional electron system.

However, in the dot-sample pronounced capacitance maxima are observed in the sub-threshold regime. As will be further verified in the following we associate the two peaks observed in this regime with the charging of the two lowest quantum levels in the quantum dots[16]. We expect the lowest s-like energy state of the quantum dots to be twofold spin degenerate and the next level to be p-like and fourfold degenerate due to the lens-shape of the InGaAs islands. Maxima arise in the capacitance signal if charge exchange between the dots and the back electrode is energetically favourable, i. e. if the total energies of the system with N and $N+1$ electrons in quantum dots are degenerate. In a simple but widely pursued model[31] the total energy of electron systems in the quantum dots is divided into a sum of two contributions one regarding the single-particle level spacing due to the size quantization of non-interacting electrons and a second term considering the Coulomb interaction of the electrons. We estimate values for these two contributions from independent measurements and determine from these the expected voltage spacing of the capacitance peaks.

The single-particle level spacing between the two lowest quantum states is determined from FIR resonances of the quantum dots measured with conventional Fourier-transform spectroscopy[16]. Assuming that the collective contributions to the resonance energy is negligible in dots occupied with very few electrons we obtain a level spacing of 41 meV. The Coulomb energy of the electrons in the dot is estimated from the self-capacitance $C = 4\epsilon\epsilon_0 d$ of a disc-shaped electrode with diameter d=20 nm as determined from the AFM or TEM inspections: $e^2/C = 18$ meV. With these energies we calculate the voltages, at which charge exchange between the dots and the back electrodes takes place and thus an increased capacitance is expected. In Fig. 11a and 11b we present experimental spectra and results of such a model calculation, respectively. For comparison with the experimental spectra in Fig. 11b a phenomenological broadening is introduced. Broadening is expected to mainly result from fluctuations of the threshold voltages of different dots in the sample[16].

The only parameters adjusted for comparison between the experimental spectra and the modelled capacitance is the center value and the width of a Gaussian distribution accounting for the distribution of the threshold voltages of the probed dots. Whereas a small broadening of 5 mV width would make the charging with every single electron discernible the experimental spectra are better described with a broadening of 25 mV, where the Coulomb energy is not resolved any more. The resolved maxima reflect the size quantization into the twofold and fourfold degenerate dot levels and their separation describes surprisingly well the separation of the capacitance maxima in the experimental spectra. Fulthermore, the magnetic field dependence calculated in our simple model accounts well for the behavior of the experimental data. As apparent in Fig.11 the p-level splits into two branches while the s-level is hardly affected by the magnetic field. Again, for the sake of simplicity we estimate the magnetic field dispersion of the energy levels in the dot from a parabolic confinement model. In Fig. 11b the separation of the branches from the s-level is calculated according to the harmonic oscillator potential model: $0.5\hbar(\sqrt{4\Omega_0^2+\omega_c^2} \pm \omega_c)$ with $\hbar\Omega_0 = 41$ meV and no further adjustable parameter.

The experiments demonstrate that we can field-effect control the number of electrons that occupy the six lowest quantum states of the InGaAs dots. Capacitance and FIR spectra provide a rather comprehensive picture about the level spacing between the

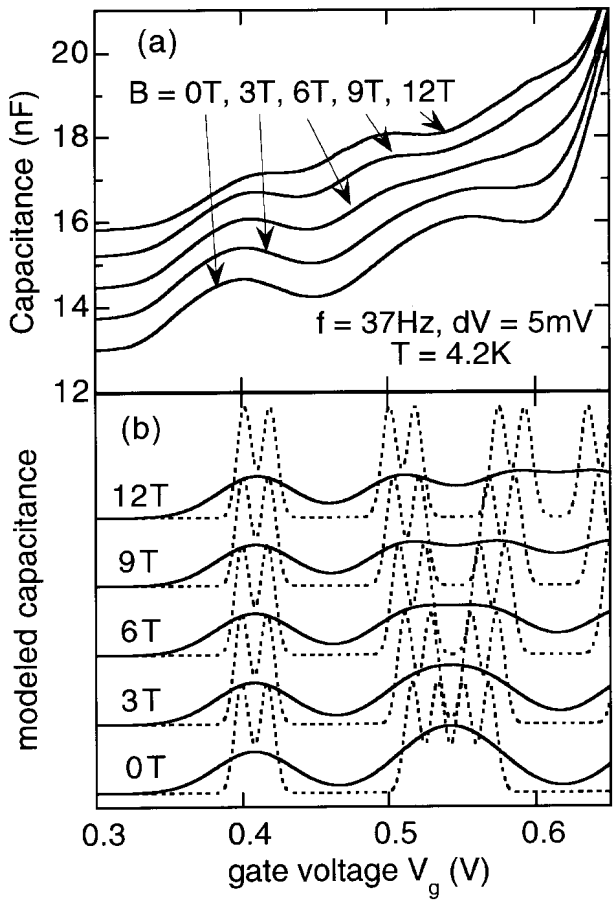

Figure 11. Experimental capacitance spectra of a MIS-diode with InGaAs quantum dots at different magnetic fields applied perpendicular to the crystal surface. The sample parameters are z_b=50 nm and z_t 95 nm as in Fig. 10. The vertical scale refers to the trace recorded at B=0, the other traces are offset for clarity (b) Capacitance traces calculated in a simple model for parameters E_{01}=41 meV and e^2/C = 18 meV. As described in the text, Gaussian broadening with standart deviations of 5 mV and 25 mV are used for the dashed and the full lines, respectively.(From Ref. [16]).

lowest energy states. A variety of experiments are presently under way that further probe the optical[32] and the electronic properties of these interesting quantum systems[33]. For example in Fig. 12 we present more recent data demonstrating that with improved growth conditions it is possible to resolve the spin degeneracy of the s-state in the charging spectra. The gate voltage regime depicted in Fig.12 retlects the subthreshold range with two capacitance maxima reflecting the charging of the s- and p-states. However, unlike in Fig.10 and Fig.11 the first maximum at V_g=0.1V exhibits a substructure indicating that it actually consists of two peaks. These we associate with the charging of the first and the second electron into the s-state. The voltage separation of the peaks is consitent with a Coulomb charging energy of 24 meV. Measurements on single self-assembled dots as well as on dot systems with controlled spatial arrangement remain to be performed in the future. Although prepared in situ during epitaxial growth without any lithography the self-assembled InGaAs quantum dots so far represent the smallest man-made zero-dimensional electron systems with a tunable number of elecIrons. If there is found a way to artificially control the location of the dots, e.g. by creation of nucleation centres, they represent very interesting systems also for possible applications[34].

IV. Summary

Very well defined electron wires and dots are field-effect induced in especially designed MIS-diodes as demonstrated by the capacitance and FIR spectra discussed in this article. With interdigital gates electron wires are investigated in the quantum limit, i.e. at electron densities where only the lowest one-dimensional subband is occupied. Parameters like the subband spacing and the one-dimensional electron density are determined in simple analytical models for the confinement potential. For the subband spacing we find typical values between 4 meV and 6 meV depending on a voltage with which we control the confinement potential.

Well resolved onset voltages for the first and the second one-dimensional subband in capacitance measurements and a narrow FIR resonance even at low electron densities in the quantum limit demonstrate the high quality of the electron systems Unlike in previous works on electron wires and dots where the structures of interest have been only resolved with a derivative technique,[35,36] here the experimental data can be more directly compared to results of more involved self-consistent model calculations. Such calculations, however, remain to be done for our devices. The elementary excitations in the wires are probed with FIR absorption experiments with a new measurement technique. This technique is very sensitive even if the wire is in the one-dimensional quantum limit. Efforts are under way to considerably reduce the length of the wire system probed in capacitance and FIR absorption experiments as is demonstrated by capacitance data obtained on a single 150 μm long wire.

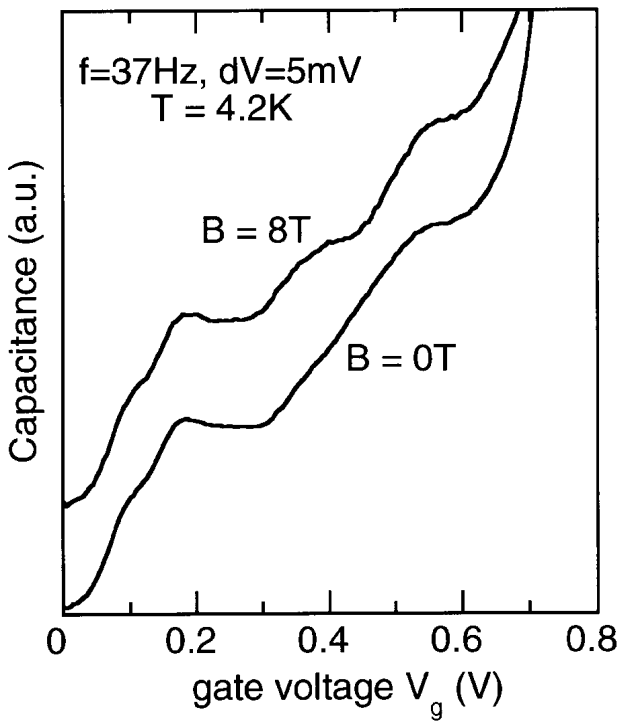

Figure 12. Experimental capacitance spectra of a sample with sufficiently small broadening to resolve the Coulomb charging of the spin degenerate lowest quantum state. The traces recorded at B=0 and 8 T are offset for clarity.

The concept of a semiconductor type I quantum dot with structurally confined electrons and holes has been realized almost ideally with self-assembled InGaAs islands grown in the Stranski-Krastanov growth mode on GaAs. Here a homogeneity at extremely small dot sizes is accomplished with relative ease that has not been accessible with lithographic techniques so far. Sandwiched in our MIS-type heterostructures between a front electrode and a back contact the electron occupation of dots can be easily controlled by a voltage. The experimental results yield a comprehensive picture of the nature of the electron quantum dots. The energy separation between the two lowest energy levels is determined to about 40 meV.

Acknowledgements

The results discussed here arise from a joint effort of three groups located in Munich, Glasgow and Santa Barbara. We are very grateful to all members of these groups who have contributed. In particular, it is a pleasure for us to acknowledge the very pleasant and fruitful collaboration with M. Holland, D. Leonard, S. Manus and A. Schmeller. M. H. and D. L. prepared the very good epitaxial heterostructure material and A. S.contributed very much to the development of the interdigital gates. S. M. helped us improving the measurement set-up and gave important hints to the interpretation of the capacitance data. Furthermore, we would like to particularly thank J. P. Kotthaus, P. M. Petroff, A. O. Govorov and V. Dolgopolov for many very valuable advises and discussions. Financial SUppOlt of the Deutsche Forschungsgemeinschaft and Esprit Basic Research is gratefully acknowledged.

References

1. T. Ando, A. B. Fowler, and F. Stern, Rev. Mod. Phys. **54**, 437 (1982).
2. C. Weisbuch and B. Vinter, *Quantum Semiconductor Structures, Fundamentals and Applications*, (Academic Press, London, 1991).
3. see e. g. *Mesoscopic Phenomena in Solids*, eds. B. L. Altshuler, P. A. Lee and R. A. Webb (North-Holland, Amsterdam, 1991): C. W. J. Beenakker and H. van Houten, in Solid State Physics Vol. **44**, eds.: H. Ehrenreich and D. Turnbull, (Academic Press, New York 1991) p. 1;*Nanostructured System, in Semiconductors and Semimetals*, ed. R. K. Williardson, A. C. Beer, E. R. Weber, Vol.**35**, ed. M. Reed, (Academic Press, San Diego 1992).
4. W. Hansen, U. Merkt and J. P. Kotthaus, in *Semiconductors and Semimetals*, ed. R. K. Williardson, A. C. Beer, E. R. Weber, Vol. 35, ed. M. Reed, (Academic Press, San Diego 1992) p. 279.
5. T. P. Smith, B. B. Goldberg, P. J. Stiles and M. Heiblum, Phys. Rev. **B32**, 2696 (1985).
6. T. P. Smith, III, W. I. Wang and P. J. Stiles, Phys. Rev. **B34**, 2995 (1986).
7. J. P. Eisenstein, L. N. Pfeiffer and K. W. West, Phys. Rev. Lett. **68**, 674 (1992).
8. S. V. Kravchenko, D. A. Rinberg and S. G. Semenchinsky, Phys. Rev. **B42**, 3741 (1990).
9. H. Drexler, W. Hansen, J. P. Kotthaus, M. Holland and S. P. Beaumont, Semicond. Sci. Techn. **7**, 1008 (1992).
10. H. L. Stormer, R. Dingle, A. C. Gossard, W. Wiegmann and M. D. Sturge, J. Vac. Sci. Technol. **16**, 1517 (1979).

11. John A. Nixon and J. H. Davies, Phys. Rev. **B41**, 7929 (1990).
12. J. H. Davies and I. A. Larkin, Phys. Rev. **B49**, 4800 (1994).
13. M. Chen, W. Porod and D. J. Kirkner, J. Appl. Phys. **75**, 2545 (1994).
14. H. Drexler, W. Hansen, A. Schmeller, J.P. Kotthaus, M. Holland and S.P. Beaumont, Solid State Electronics **37**, 1289 (1994).
15. D. Leonard, M. Klishnamurthy, C.M. Reaves, S.P. Denbaars, P.M. Petroff, Appl. Phys. Lett. **63**, 3203, (1993).
16. H. Drexler, D. Leonard, W. Hansen, J.P. Kotthaus, P.M. Petroff, Phys. Rev. Lett. **73**, 2252 (1994).
17. D. Leonard, K. Pond and P. M. Petroff, Phys. Rev. **B50**, 11687 (1994).
18. H. Drexler, W. Hansen, S. Manus, J. P. Kotthaus, M. Holland and S. P. Beaumont, Phys. Rev. **B 49**, 14074 (1994).
19. W. Hansen in *Festkörperprobleme*, Advances in Solid State Physics Vol. 35, ed. by R. Helbig, in press.
20. R. C. Ashoori, H. L. Stormer, J. S. Weiner, L. N. Pleiffer, K. W. Baldwin and K. W. West, Phys. Rev. Lett. **71**, 613 (1993).
21. D. Schmerek, unpublished.
22. A. O. Govorov, unpublished.
23. W. Hansen, in *Physics of Nanostructures*, eds. J. H. Davies and D. A. Long (SUSSP and IOP, Bristol 1992), p. 257.
24. H. Drexler, W. Hansen, J. P. Kotthaus, M. Holland and S. P. Beaumont, Appl. Phys. Lett. **64**, 227() (1994).
25. W. Kohn, Phys. Rev. **123,** 1242 (1961).
26. L. Brey, N. F. Johnson and B. I. Halperin, Phys. Rev. **B40**, 10647 (1989). Technol. **7**, 1008 (1992).
27. W. Que, Phys. Rev. **B43**, 7127, (1991).
28. Drexler, W. Hansen, J. P. Kotthaus, M. Holland and S. P. Beaumont, Phys. Rev. **B46**, 12849 (1992).
29. V. Gudmundsson, A. Brataas, P. Grambow, B. Meurer, T. Kurth and D. Heitmann, Phys. Rev. B, in press.
30. L. Wendler and V. G. Grigoryan, unpublished.
31. H. van Houten, C. W. J. Beenakker and A. A. M. Staring in Single Charge Tunneling, ed. by H. Grabert and M. H. Devoret (Plenum Press, 1992).
32. J.-Y. Marzin, J.-M. Gerard, A. Izrael, D. Barrier and G. Bastard, Phys. Rev. Lett. **73**, 716 (1994).
33. G. Medeiros-Ribeiro. D. Leonard, P.M. Petroff, Appl. Phys. Lett.**66**, 1767 (1995).
34. C. S. Lent, P. Douglas Tougaw and W. Porod, Appl. Phys. Lett. **62**, 714 (1993).
35. T. P. Smith, III, H. Arnot, J. M. Hong, C. M. Knoedler, S. E. Laux and H. Schmid, Phys. Rev. Lett. **59**, 2802 (1987).